Design and Operation of a Supersonic Annular Flow Facility

K. E. Williams* and F. B. Gessner†
University of Washington, Seattle, Washington 98195
and
G. J. Harloff‡
Sverdrup Technology, Inc., Brook Park, Ohio 44142

Introduction

SUPERSONIC annular flow passages exist in propulsion applications that include dual combustion ramjet engines where a supersonic annular flow (the outer flow) mixes with a sonic (or supersonic) gas generator flow (the inner flow) in the shock expansion zone downstream of the gas generator nozzle exit.[1] Other engine designs include components in the form of annular ducts whose cross-sectional area varies in the streamwise flow direction. In some of these configurations, it is necessary to support the outer shroud (cowl) by means of struts positioned between the cowl and centerbody. To investigate the distorting influence of these struts on the local flow structure, it is first necessary to ensure that the intrinsic flow without struts is free of wave reflections and the effects of upstream disturbances. It is also necessary to demonstrate that the intrinsic flow exhibits the characteristics of a well-defined turbulent boundary-layer flow, so that changes in the local flow structure induced by the presence of struts can be interpreted properly. The purpose of this Note is to demonstrate that a supersonic flow facility that meets these objectives has been developed.

Experimental Program

To generate a supersonic annular duct flow, a new continuous flow facility was designed consisting of a plenum chamber, annular nozzle, test section, and downstream ductwork connected to a large vacuum tank. This facility was built at the University of Washington and is located in the Heat Power Laboratory. High-pressure air enters the plenum chamber through an inlet piping configuration and porous filter as shown in Fig. 1a. Low-pressure air is evacuated continuously from the vacuum tank by means of a Nash liquid ring vacuum pump and four Worthington steam ejectors. The polished aluminum centerbody that forms the inner wall of the annulus was designed to slide within a stationary steel cylindrical sleeve, so that struts mounted on the centerbody in future experiments could be positioned at different distances relative to the nozzle exit. The cylindrical sleeve is held in position by two sets of four positioning screws, circumferentially spaced 90 deg apart. The first set is located directly behind the main inlet pipe flange in Fig. 1a. The second set is located at approximately the midlength of the plenum and works against a shroud (inner ring) connected to four airfoil-shaped (elliptic cross section) struts attached to the cylindrical sleeve. This strut configuration is rotated 45 deg relative to the vertical plane of the plenum, as shown in Fig. 1a. By adjusting both sets of positioning screws, the centerbody could be positioned concentrically within the convergent-divergent nozzle mounted on the discharge side of the plenum to within an estimated accuracy of ±0.05 mm (±0.002 in.) relative to a throat gap width of 4.82 mm (0.190 in.). A hexagonal aluminum honeycomb with individual cells 6.4 mm (0.25 in.) wide and a 16 × 16 mesh brass screen were located between the elliptic strut array and nozzle inlet to minimize the circumferential flow distortion induced by the struts and to break up any large-scale vortical structures in the flow.

A schematic diagram of the annular nozzle and test section downstream of the plenum is shown in Fig. 1b. The contoured section of the nozzle and the outer wall of the test section were machined from 178 mm (7.000 in.) diam. solid Plexiglas® rod, and the interior surfaces were polished. The nozzle was designed by applying the method of characteristics to determine the outer wall contour downstream of the throat. This was done without accounting for viscous boundary-layer development on the inner (centerbody) and outer walls. After the coordinates for the diverging wall contour had been determined, the coordinates near the throat were fitted to a parabolic profile matched to the radius of curvature at the throat. The parabolic profile was continued upstream until the angle of the convergent wall was 45 deg relative to the axial centerline of the nozzle. At this point the outer wall of the nozzle was continued outward at a 45-deg angle until just before the plenum wall where the outer wall was contoured to create a smooth transition from the constant radius plenum wall to the nozzle contraction. The pertinent coordinates relative to the nozzle are shown in Fig. 1b where x_t and x are axial coordinates measured from the nozzle throat and exit, respectively, and $x_c = 0$ denotes the axial location in the plenum where numerical computations were begun. The nozzle was designed to yield a nominal core flow Mach number of 3.0 at the nozzle

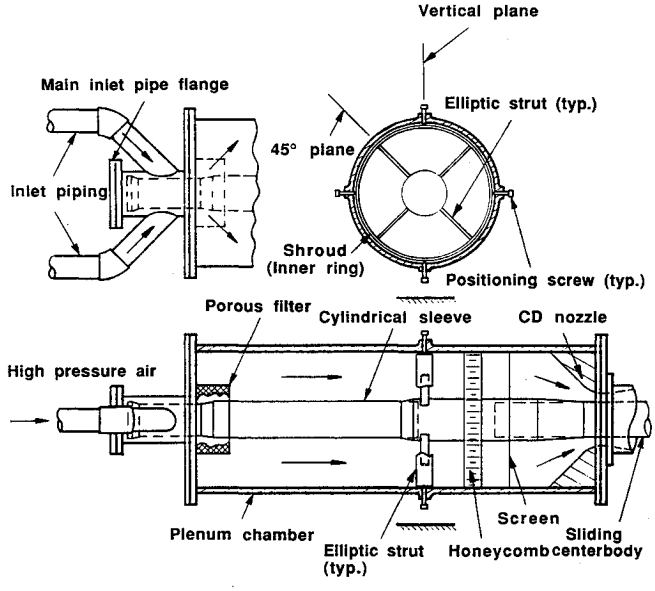

a) Configuration upstream of nozzle

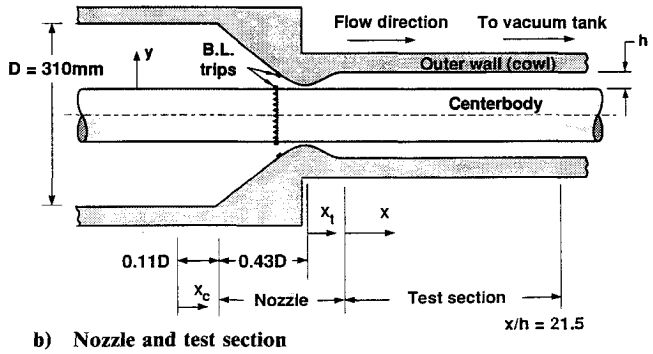

b) Nozzle and test section

Fig. 1 Plenum configuration, nozzle, and test section with pertinent dimensions and coordinates.

Presented as Paper 93-3123 at the AIAA 24th Fluid Dynamics Conference, Orlando, FL, July 6-9, 1993; received July 8, 1993; revision received Feb. 1, 1994; accepted for publication Feb. 2, 1994.

*Graduate Research Associate, Department of Mechanical Engineering. Student Member AIAA.
†Professor, Department of Mechanical Engineering. Member AIAA.
‡Senior Staff Scientist, LeRC Group; currently at NYMA, Inc., Brook Park, OH. Associate Fellow AIAA.

exit where the Reynolds number based on gap width was 2.4×10^5 for the maximum operating plenum pressure of 1030 mmHg (19.9 psia). The centerbody diameter was constant at 83.0 mm (3.267 in.), and the ratio of centerbody-to-outer-wall radius was fixed at 0.7. This yielded an annular gap width h of 17.8 mm (0.700 in.) that was constant along the length of the test section. The inner and outer wall boundary layers were tripped near the throat of the nozzle by mounting a ring of triangular-shaped elements on each surface with apexes facing forward, as suggested by Chou and Childs.[2] The trips were made from 100 grit garnet paper, 0.38 mm (0.015 in.) thick; additional details of the trip configuration are given by Williams.[3]

To examine the quality of the flow, wall static pressure distributions were measured by means of taps on the centerbody and outer wall having an orifice diameter of 0.34 mm (0.0135 in.). A conical probe with a tip diameter of 1.07 mm (0.042 in.) and side holes based on the design recommendations of Chue[4] was used to measure static pressure in the core flow. Two miniature circular pitot probes, one with a tip canted toward the centerbody and the other with a tip canted toward the outer wall, were used to measure pitot pressure profiles. Each probe was made of nested stainless steel tubing terminating in a 0.30 mm (0.012 in.) diameter tip exposed to the flow. The pressure probe data were used to evaluate Mach number profiles and axial mean velocity profiles at four streamwise locations downstream of the nozzle exit (at $x/h = 3.6$, 5.7, 8.6, and 11.4) for assumed adiabatic wall conditions. The local wall shear stress was determined by means of four different diameter, circular pitot tubes resting on the wall (Preston tubes). For measurements on both the centerbody and outer walls, probes with outside diameters of 0.064, 1.07, 1.65, and 2.11 mm (0.025, 0.042, 0.065, and 0.083 in.) were used. Only data that satisfied the minimum and maximum probe diameter criteria set forth by Allen[5] were used to calculate the local skin friction. When this restriction was applied, local skin friction values on each surface at a given location agreed to within ±2.2% of the average value calculated from the Preston tube data reduction formula proposed by Hopkins and Keener.[6] Further details of the data reduction procedures, tunnel operation, instrumentation, and overall flow facility are given by Williams.[3]

Numerical Approach

For purposes of comparison with the experimental results, numerical computations were performed using the PARC-3D flow code[7] that solves the Reynolds-averaged equations of motion in strong conservation form using the Beam and Warming approximate factorization algorithm. Closure to the equations of motion was effected by incorporating the Baldwin-Lomax turbulence model[8] into the code. The computations were initiated in the plenum chamber at $x_c = 0$ (refer to Fig. 1) where a low-turbulence-level, subsonic uniform mean flow was assumed. Wall boundary conditions were specified consistent with the physical geometry of the plenum, nozzle, and test section. Outflow properties were extrapolated at the outflow plane of the test section, and adiabatic wall conditions were assumed. The computations were performed for a circumferentially symmetric flow using a 237×99 grid. The 237 grid points in the x direction were clustered near the throat and extended from $x_c = 0$ to the outflow plane (at $x/h = 21.5$). A hyperbolic clustering function was used to locate the first grid point near each wall at a y^+ value less than unity, which enabled the local skin friction to be evaluated directly from the axial velocity gradient at the wall.

Results and Discussion

Initial data were taken for a plenum pressure of 800 mmHg to investigate the effect of boundary-layer trip location on Mach number profiles measured in the duct downstream of the nozzle exit. Figure 2 shows centerbody Mach number profiles measured at $x/h = 3.6$ with the centerbody trip positioned sequentially at four locations upstream of the nozzle throat. Also shown in this figure are values of the acceleration parameter $[K \equiv (\nu_w/U_e^2)\, dU_e/dx]$ where U_e was evaluated by assuming inviscid flow in the converging annular section upstream of the nozzle throat. From the figure it can be seen that the two profiles measured with the trip positioned at $x_t = -41$ mm and then at -18 mm are indicative of laminar or transitional-like behavior in that relatively low Mach number (momentum flux) levels exist near the wall and the boundary-layer thickness is relatively thin. This behavior indicates that the flow either relaminarized or that complete transition to turbulent flow did not occur with the trip positioned at either of these two locations. In contrast, when the centerbody trip was repositioned at $x_t = -13$ mm and then at -8 mm, Fig. 2 shows that Mach number profiles measured at $x/h = 3.6$ for these two trip positions are essentially coincident and indicative of fully turbulent behavior. A plot of the corresponding velocity profiles in law-of-the-wall coordinates confirmed this to be the case. The results in Fig. 2 imply that sustained turbulent flow existed downstream of the trip when the trip was positioned upstream of the throat at a streamwise location where $K \leq 3.5 \times 10^{-6}$. This value is close to the relaminarization limit cited by Kline et al.,[9] namely, $K = 3.7 \times 10^{-6}$, above which turbulent bursts in the wall boundary layers they investigated were completely suppressed. This limit is, however, higher than typical values based on the relaminarization correlation proposed by Nash-Webber and Oates,[10] whose results indicate that relaminarization will generally occur whenever $K \geq 1 \times 10^{-6}$ to 2×10^{-6}, depending on the magnitude of the momentum thickness Reynolds number. In the present study, K remained below 3.5×10^{-6} along the length of the nozzle downstream of the centerbody trip at $x_t = -13$ mm. Under these conditions, vorticity introduced into the boundary layer at the trip location was apparently not suppressed, and normal turbulent boundary-layer development occurred on the centerbody without relaminarization. On the basis of these results, trips were positioned on both the nozzle and centerbody walls at $x_t = -13$ mm, and all subsequent data were taken for this operating condition. The plenum pressure was also raised from 800 to 1030 mmHg to increase the operating Reynolds number and minimize the possibility of incomplete transition.

Static pressure distributions in the annular duct (test section) indicated that weak oblique wave reflections were present in both the experimental and numerical flows as a result of incomplete Mach wave cancellation on the nozzle surface near the nozzle exit. Computed and measured Mach number profiles were relatively insensitive to this effect, however, as

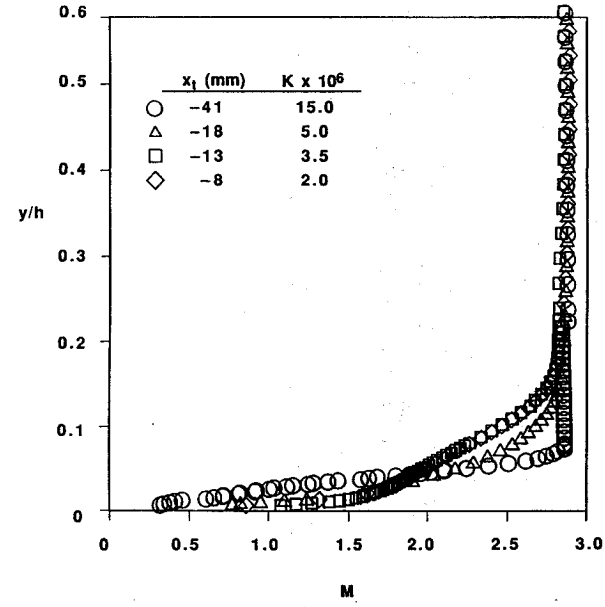

Fig. 2 Effect of boundary-layer trip location on centerbody Mach number profiles measured at $x/h = 3.6$ and $P_t = 800$ mmHg.

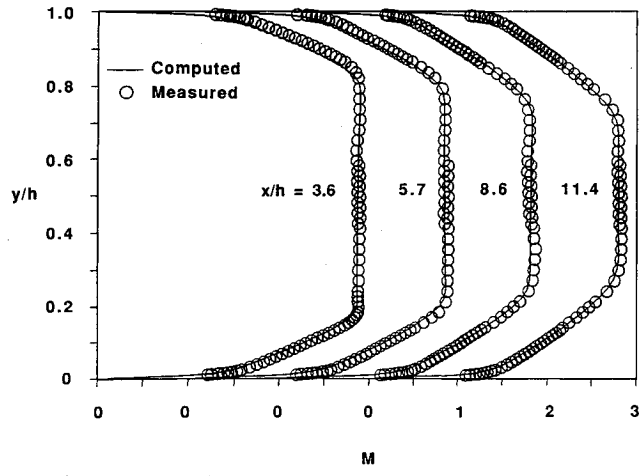

Fig. 3 Computed and measured Mach number profiles.

can be seen by referring to the results in Fig. 3, which show no observable manifestation of wave distortion. The level of agreement between the computed and measured Mach number profiles in Fig. 3 is, in fact, rather remarkable, given the different streamwise development histories of the two flows. The numerical computations were initiated in the plenum chamber upstream of the nozzle and were performed before the experimental facility was built. The Baldwin-Lomax turbulence model was applied over the entire development length of the numerical flow between the plenum and test section outlet, so that fully turbulent boundary-layer flow was present, even in regions where acceleration effects led to relaminarization of the experimental flow. The trips used in the experimental flow also caused the wall boundary layers upstream of the nozzle throat to thicken more rapidly in a region where the boundary layers of the numerical flow were changing more gradually. Some insight into possible reasons for the high level of agreement between the computed and measured results in Fig. 3 can be gleaned by first noting that the thickness of the nozzle and centerbody boundary layers was significantly reduced as the experimental and numerical flows were accelerated between the experimental trip location and the nozzle throat. As a result, the virtual origins of the nozzle and centerbody boundary layers were located relatively close to the throat for both flows. If the experimental and numerical boundary-layer flows on each wall originated from essentially the same virtual origin, and the prescribed turbulence model was appropriate, then one would expect similar boundary-layer growth patterns for both flows downstream of the virtual origin. This would explain the high level of agreement between corresponding profiles in Fig. 3. It should not be inferred from this conjectured behavior, however, that specifying uniform flow with zero boundary-layer thickness at the nozzle throat offers an acceptable alternative to initiating the computations in the plenum chamber. The present computations show that although the boundary-layer thickness on the centerbody and outer walls is relatively thin at the nozzle throat ($\delta_{cb} \cong \delta_{ow} \cong 0.00044\ h_t$ where h_t is the throat gap width), core flow static pressure and Mach number vary by approximately 7% with radial position in the inviscid region of the flow, which precludes specification of uniform flow at the nozzle throat as a valid starting condition.

As a further test of compatibility between the experimental and numerical flows, axial velocity profiles were evaluated at the four streamwise locations shown in Fig. 3. Results for the centerbody and outer wall velocity profiles are shown in Fig. 4 in terms of van Driest scaled variables. From the figure it can be seen that computed and measured U^+ profiles on each surface agree well at all four streamwise locations. The computed profiles mimic the linear relationship $U^+ = y^+$ in the viscous sublayer ($0 < y^+ \leq 5$), and both sets of profiles agree well with the law of the wall within the interval $30 \leq y^+ \leq 100$.

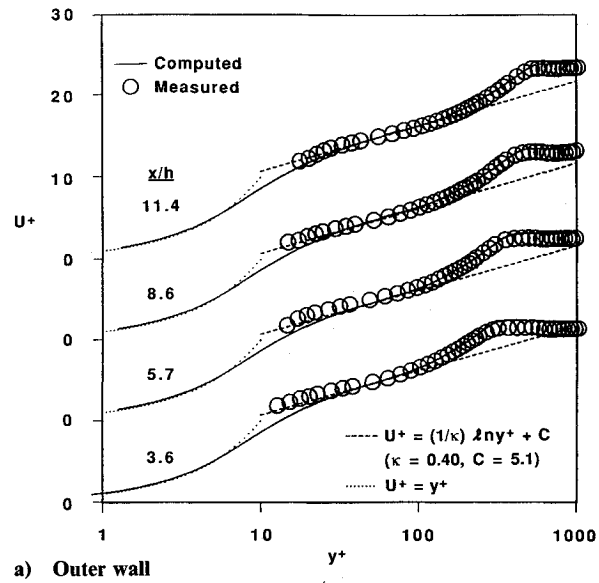

a) Outer wall

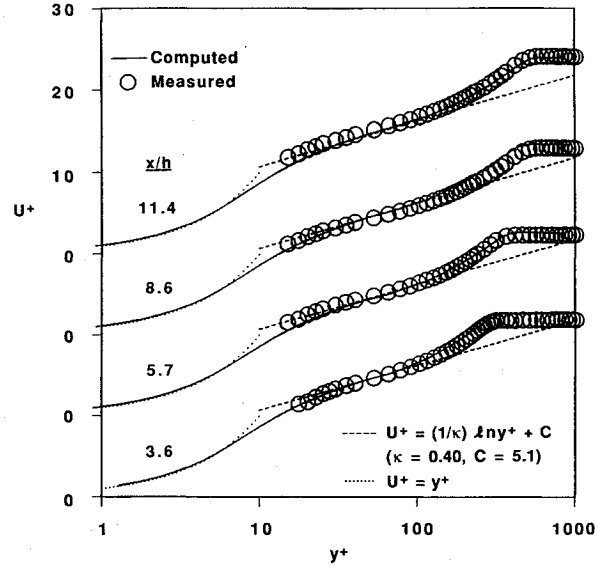

b) Centerbody

Fig. 4 Computed and measured axial velocity profiles in law-of-the-wall coordinates.

On the basis of the results shown in Figs. 3 and 4, it is apparent that both the centerbody and outer wall boundary layers exhibit the characteristics of a well-defined turbulent boundary layer and that no adjustments need to be made to either the experimental or computed flow to insure matched flow conditions at any streamwise location within the annular duct test section.

Concluding Remarks

In this Note several important issues have been addressed as they relate to shock-free, supersonic turbulent flow in an annular duct. By properly designing the flow components upstream of the duct and choosing an appropriate boundary-layer trip location, it has been shown that an experimental flow can be generated for which the inner and outer wall boundary layers are fully turbulent, with the near-wall flow in local equilibrium at all streamwise locations along the duct. By initiating the computations in the plenum chamber and prescribing the Baldwin-Lomax turbulence model, it has been shown that excellent agreement is possible between the experimental and numerical flows. As a result, initial conditions can be prescribed properly for the computation of shock-wave/boundary-layer interaction phenomena induced by struts placed

between the duct walls. Experimental and numerical studies of these phenomena will be the subject of future research.

Acknowledgment

The authors would like to express their appreciation to the NASA Lewis Research Center, which supported this work under Grant NAG3-376 and Contract NAS3-25266.

References

[1]Stockbridge, R. D., "Experimental Investigation of Shock Wave/Boundary-Layer Interactions in an Annular Duct," *Journal of Propulsion and Power,* Vol. 5, No. 3, 1989, pp. 346–352.

[2]Chou, J.-H., and Childs, M. E., "A Study of the Effects of Trips on Compressible Boundary Layers," Dept. of Mechanical Engineering, Univ. of Washington, Rept. TR78-SW-8-1, Seattle, WA, Aug. 1978.

[3]Williams, K. E., "Design and Preliminary Measurements in a Supersonic Strut-Endwall Flow Facility," M.S. Thesis, Dept. of Mechanical Engineering, Univ. of Washington, Seattle, WA, Oct. 1991.

[4]Chue, S. H., "Pressure Probes for Fluid Measurement," *Progress in Aerospace Sciences,* Vol. 16, No. 2, 1975, pp. 147–223.

[5]Allen, J. M., "Critical Preston-Tube Sizes," *Journal of Aircraft,* Vol. 7, No. 3, 1970, pp. 285–287.

[6]Hopkins, E. J., and Keener, E. R., "Study of Surface Pitots for Measuring Turbulent Skin Friction at Supersonic Mach Numbers-Adiabatic Wall," NASA TN D-3478, July 1966.

[7]Cooper, G. K., and Sirbaugh, J. R., "PARC Code: Theory and Usage," Arnold Engineering Development Center, AEDC-TR-89-15, Arnold Air Force Base, TN, Dec. 1989.

[8]Baldwin, B. S., and Lomax, H., "Thin Layer Approximation and Algebraic Model for Separated Turbulent Flows," AIAA Paper 78-257, Jan. 1978.

[9]Kline, S. J., Reynolds, W. C., Schraub, F. A., and Runstadler, P. W., "The Structure of Turbulent Boundary Layers," *Journal of Fluid Mechanics,* Vol. 30, Pt. 4, 1967, pp. 741–773.

[10]Nash-Webber, J. L., and Oates, G. C., "An Engineering Approach to the Design of Laminarizing Nozzle Flows," *Journal of Basic Engineering,* Vol. 94, No. 4, 1972, pp. 897–904.

Model for Compressible Turbulence in Hypersonic Wall Boundary and High-Speed Mixing Layers

Rodney D. W. Bowersox*
Air Force Institute of Technology,
Wright-Patterson Air Force Base, Ohio 45433
and
Joseph A. Schetz†
Virginia Polytechnic Institute and State University,
Blacksburg, Virginia 24061

Introduction

THE most common approach to Navier-Stokes predictions of turbulent flows is based on either the classical Reynolds- or Favre-averaged Navier-Stokes equations or some combination.[1–3] Wilcox[4] suggests two research avenues for arriving at turbulence models suitable for hypersonic flows: 1) develop new models, or 2) generalize existing models. Wilcox,[4] as well as other researchers, have made great strides in the latter. As discussed by Wilcox, virtually all generalized models assume that Morkovin's hypothesis applies, which may become questionable for hypersonic boundary layers and high-speed free mixing layers. The present study addressed relaxing Morkovin's hypotheses by directly accounting for the density-velocity fluctuation correlation in the conservation equations of mass, momentum, and energy. The experimental results discussed later support this new ideology.

Mikulla and Horstman[5] present cross-wire measurements in a Mach 7 boundary layer. These data along with corollary data[6,7] were "re-reduced" here, using typical methods,[8] into the results given in Fig. 1a. The incompressible term of the Reynolds shear stress (Fig. 1a, open circles) only accounted for about 30% of the total turbulent shear stress (open triangles), and the compressible term (open squares) contributed the remaining 70%. Bowersox and Schetz[8] found that, for a Mach 4.0 free mixing layer, the incompressible shear term only accounted for about 25% (Fig. 2a, open circles) of the total shear stress (open triangles), whereas the compressible terms (open squares) contributed the remaining 75%.

The main goal of the current work was to numerically assess the effects of the compressible turbulence terms that were experimentally found to be important. The compressible apparent mass mixing length extension (CAMMLE) model,[8] which was based on measured experimental data (Figs. 1a and 2a, solid symbols), was found to produce accurate predictions of the measured compressible turbulence data for both the wall bounded and free mixing layer. Hence, that model was incorporated into a finite volume Navier-Stokes code.

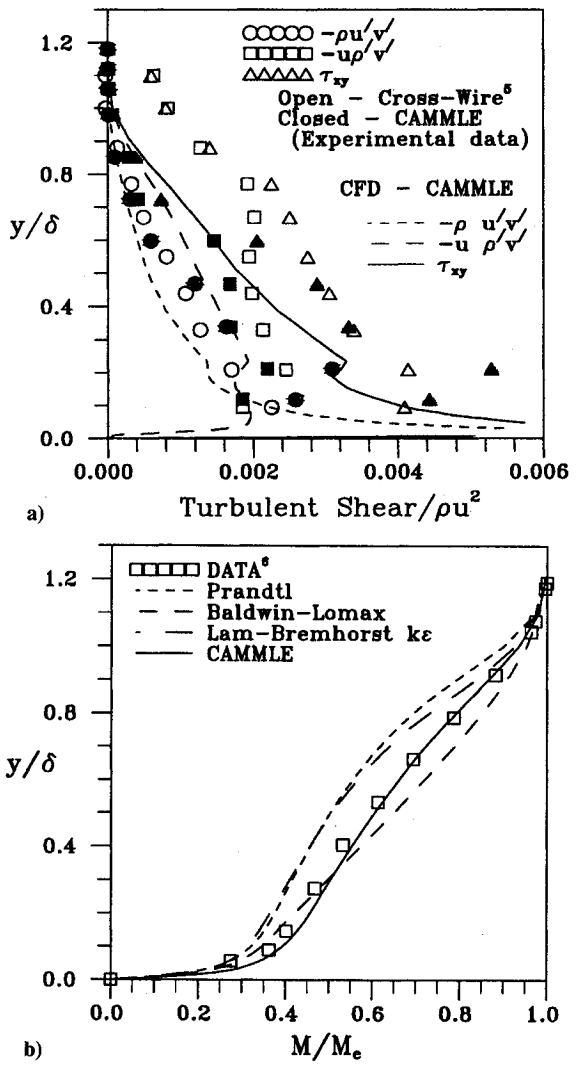

Fig. 1 Mach 6.85 (Refs. 5–7) experimental and numerical boundary-layer comparisons (x = 237 cm): a) Reynolds shear stress profiles (open symbols, cross-wire measurements; closed symbols, CAMMLE[8] model results evaluated with measured mean flow data; and lines, numerical CAMMLE results) and b) Mach number profile (symbols, measurements; and lines, numerical predictions).

Presented as Paper 93-2904 at the AIAA 24th Fluid Dynamics, Plasmadynamics, and Lasers Conference, Orlando, FL, July 6–9, 1993; received Oct. 23, 1993; revision received Jan. 6, 1994; accepted for publication Jan. 22, 1994.

*Assistant Professor, Department of Aeronautical and Astronautical Engineering. Member AIAA.

†J. Byron Maupin Professor, Department of Aerospace and Ocean Engineering. Fellow AIAA.